

Neutral Stability Curves for plane Poiseuille, Blasius Boundary-Layer and Falkner-Skan Flows

Shigenobu Itoh

February 11, 2017

abstract Neutral stability curves for plane Poiseuille flow, laminar boundary-layer flow and Falkner-Skan flow were obtained numerically and showed that there is a local minimum-maximum (or a kink) on the upper branch of the curve. For the plane Poiseuille flow, the method related to Spectral methods was used, and for the boundary-layer flow and for the Falkner-Skan flow in the semi-infinite regions, the flows were mapped to each finite region, and the above-described method was applied to those flows. The above-mentioned method related to Spectral methods is a method which discretizes the direction perpendicular to the flow and replaces the differential operators in the Orr-Sommerfeld equation with the Chebyshev Differentiation Matrices at those discrete points, thereby reducing the whole to the generalized eigenvalue problems. Here, Scilab freeware-solver was used for numerical solution of generalized eigenvalue problem.

1 Introduction

Whether or not the main flow having the velocity $\mathbf{U}(\mathbf{x})$ is stable can be determined by adding an infinitesimally small disturbance $\hat{\mathbf{u}}$ to the main-flow-velocity \mathbf{U} . That is, if the disturbance $\hat{\mathbf{u}}$ increases with time, the main flow \mathbf{U} is unstable, whereas if the disturbance $\hat{\mathbf{u}}$ disappears, the main flow \mathbf{U} is stable. The Orr-Sommerfeld equation [1] (hereinafter referred to as O-S equation) is an equation that formulated this idea. If disturbance \mathbf{u} does not grow or disappear with time, it is called a neutral stable state.

The (R, α) plane is divided into a stable region and an unstable region by an O-S equation with the wave number α and the Reynolds number R as parameters, and the boundary between the two regions becomes a neutral stability curve. Therefore the purpose of this paper is to find this curve for the flow of the flat Poiseuille flow, flat boundary layer flow and Falkner-Skan equation[2].

In order to obtain a neutral stability curve, we use the differential operator-matrix: “Chebyshev Differentiation Matrix” [3] (hereinafter abbreviated as CDM) related to the spectral method. The procedure is first to discretize the direction orthogonal to the flow direction in the O-S equation, to further replace the derivative inside the equation with CDM, to derive matrix-type equations, and to reduce this matrix equation to the generalized eigenvalue problem. Find the point where the sign of the imaginary part of the eigenvalue obtained changes, and find the neutral stability curve of Poiseuille flow and boundary layer flow. Numerical solution of

these series of eigenvalue problems was done by freeware Scilab.

According to this method, a numerically exact curve can be obtained for the neutral stability curve of Poiseuille flow between a finite distance generated by two plates. Whereas in the case of the boundary layer flow on the flat plate, the direction perpendicular to the flow on the flat plate extends infinitely. Therefore in order to adapt to this CDM method, it is necessary to this infinite area be mapped to the finite bounded area.

For these neutral stability curves, a local minimum maximum occurs in the upper-branch of the curve, which is also pointed out in Healey's paper[4]. In his paper, he called the local minimum maximum as kink, which can be related to small loops surrounding the singularity of the Tietjens function used in finding the curve, but it is regarded as a robust feature that appears in a wide range of stability problems.

By the way, Schlichting also studied the case where there is a positive pressure gradient in the flow outside the boundary layer in Chapter 17 of the above-mentioned document, and the velocity profile of this boundary layer flow is a flow having inflection points and he showed the following points. Schlichting approximates the boundary layer flow with the inflection point by a sixth degree polynomial, and a neutral stability curve for this flow was obtained. On the other hand, the flow represented by the Falkner-Skan equation, which is considered to be a general boundary layer flow, becomes a flow having an inflection point as well as a flow having no inflection point depending on the parameters in the equation. If we use a solution with this inflection point, we can discuss more accurate neutral stability curves, unlike Schlichting's approximate solution. From this standpoint, Wazzan et al. [5] numerically derived the neutral stability curve of Falkner-Skan flow. In this paper we discuss here again from the viewpoint including kink in the neutral stability curve.

Prior to Schlichting, Rayleigh conducted an important study on a non-viscous flow with inflection points. The equation ignoring the viscosity term from the O-S equation becomes a Rayleigh equation. Therefore, the Rayleigh equation is an equation that discusses the stability of non-viscous flow. In this paper we briefly discussed the stability from the viewpoint of eigenvalues of this equation.

We will describe the constitution of this paper. In Section 2 we introduce the O-S equation. Section 3 defines the CDM and further reduces the O-S equation to the generalized eigenvalue problem. Comparing the results of eigenvalues thus obtained with the published results, we confirm the effectiveness of our method. The method used here is the method discussed in Chapter 14 itself of Trefethen[3], but as a result of drawing a detailed neutral stability curve of the plane Poiseuille flow newly based on this method, when the Reynolds number R approaches 1×10^8 , the kink appeared. In Section 4, the same method was applied to the boundary layer flow and a neutral stability curve was obtained. As a result, the kink was captured near the Reynolds number $R = 1 \times 10^5$ defined by the displacement thickness. In Section 5, we will confirm the occurrence of the kink in neutral stability curves for various flows such as flows with inflection point in the velocity profile obtained from Falkner-Skan equation. Finally, we discuss the stability of non viscous flow with inflection point from the viewpoint of Rayleigh equation.

2 The O-S (Orr-Sommerfeld) equation

Fluid flows are governed by following the Navier-Stokes equation

$$\frac{\partial \mathbf{u}}{\partial t} + (\mathbf{u} \cdot \nabla) \mathbf{u} = -\frac{1}{\rho} \nabla p + \nu \nabla^2 \mathbf{u}, \quad (1)$$

where $\mathbf{u} = \mathbf{u}(\mathbf{x}, t)$, $p = p(\mathbf{x}, t)$, ρ and ν are the velocity, pressure, density and kinematic viscosity, respectively. Further, the fluid is assumed to be an incompressible, so $\nabla \cdot \mathbf{u} = 0$. In order to determine the stability of the flow, we introduce a small disturbance $\hat{\mathbf{u}} = (u, v, w)$ into the main stream so the total flow velocity is $\mathbf{u} = \mathbf{U} + \hat{\mathbf{u}}$. Here \mathbf{U} is a main flow and is restricted further to

$$\mathbf{U}(\mathbf{x}) = (U(y), 0, 0). \quad (2)$$

Substitute the main-flow \mathbf{U} of this form into the velocity $\mathbf{u} = \mathbf{U} + \hat{\mathbf{u}}$, and substitute this velocity into (1), then apply $\nabla \times$ twice, and ignore the square of the infinitesimally small disturbance, etc. After a slight troublesome procedure, the y component of the equation becomes an equation of only v , that is

$$\left(\frac{\partial}{\partial t} + U \frac{\partial}{\partial x} \right) \nabla^2 v - \frac{d^2 U}{dy^2} \frac{\partial v}{\partial x} - \nu \nabla^4 v = 0. \quad (3)$$

Here, we introduce the following dimensionless quantities using the typical length \mathcal{L} and representative speed U_0 to make the whole dimension non-dimensional:

$$\bar{x} = \frac{x}{\mathcal{L}}, \quad \bar{y} = \frac{y}{\mathcal{L}}, \quad \bar{z} = \frac{z}{\mathcal{L}}, \quad \bar{t} = \frac{U_0}{\mathcal{L}} t, \quad \bar{U}(\bar{y}) = \frac{U}{U_0}, \quad (4)$$

So far we have considered the three dimensional flow, but according to Squire's theorem (see[1] § 2.4), we know that it is only necessary to first consider the two-dimensional case. Therefore, we consider a two-dimensional disturbance with $\hat{\mathbf{u}} = (u, v)$ for small disturbance.

We assume that the dimensionless y component of the disturbance, $\bar{v} = v/U_0$, is periodic in the \bar{x} , so that $\bar{v} \propto e^{i\alpha\bar{x}}$, and also assume that $\bar{v} \propto e^{-i\alpha c\bar{t}}$ for time. Where α is a dimensionless wave number and c is a complex number to be defined later. Furthermore, when the \bar{y} directional dependence of v is represented by $\phi(\bar{y})$, it becomes finally $\bar{v} = \phi(\bar{y})e^{i\alpha(\bar{x}-c\bar{t})}$. Thus, considering the dimensionless quantity of (4) and expressing (3), we obtain the following O-S equation :

$$ia \left[(\bar{U} - c) \left(\frac{d^2}{d\bar{y}^2} - \alpha^2 \right) - \frac{d^2 \bar{U}}{d\bar{y}^2} \right] \phi - \frac{1}{R} \left(\frac{d^2}{d\bar{y}^2} - \alpha^2 \right)^2 \phi = 0, \quad (5)$$

where, R is the Reynolds number and is defined as $R = U_0 \mathcal{L} / \nu$. The boundary condition for ϕ is derived from the no-slip condition $v = 0$ and the incompressible condition, that is $\phi(\bar{y})$ is to satisfy the following conditions on $\bar{y} = \bar{y}_1, \bar{y}_2$:

$$\phi(\bar{y}) = \frac{d\phi(\bar{y})}{d\bar{y}} = 0. \quad (6)$$

Letting the complex number c introduced in the assumption of \bar{v} be $c = c_r + ic_i$, if the imaginary part c_i of c becomes positive, v will increase with time.

Rayleigh equation will be derived from the limit $\alpha R \rightarrow \infty$ in the equation(5)

$$\left[(\bar{U} - c) \left(\frac{d^2}{d\bar{y}^2} - \alpha^2 \right) - \frac{d^2 \bar{U}}{d\bar{y}^2} \right] \phi = 0. \quad (7)$$

The boundary conditions are $\phi(\bar{y}_1) = \phi(\bar{y}_2) = 0$.

3 Neutral stability curve for the plane Poiseuille flow

3.1 CDM (Chebyshev Differentiation Matrix)

CDM is related to the spectral (collocation) method and this CDM is described in Trefethen's "Spectral Methods in MATLAB" [3].

Allocate $N + 1$ discrete unevenly-spaced points to the interval $-1 \leq y \leq 1$ as follows:

$$y_j = \cos \frac{j\pi}{N}, \quad j = 0, 1, \dots, N \quad (8)$$

These generated points are called Gauss-Chebyshev-Lobatto points or the second type of Chebyshev points (hereinafter abbreviated as GCL points).

Given a grid function ψ_j of the function $\psi(y)$ defined on the GCL points, we obtain a discrete derivative w in two steps:

- (i) Let p be the unique polynomial of degree $\leq N$ with $p(y_j) = \psi_j$, $0 \leq j \leq N$.
- (ii) Set $w_j = p'(y_j)$ ($' \equiv d/dy$)

This operation is linear, so it can be represented by multiplication by an $(N + 1) \times (N + 1)$ matrix, which we shall denote by D_N :

$$w = D_N \psi$$

Here N is an arbitrary positive integer, even or odd. The matrix D_N is called CDM[3]. The entries of this matrix are :

$$\begin{aligned} D_{00} &= \frac{2N^2 + 1}{6}, \quad D_{NN} = -\frac{2N^2 + 1}{6}, \\ D_{ii} &= \frac{-y_i}{2(1 - y_i^2)}, \quad i = 1, \dots, N - 1, \\ D_{ij} &= \frac{c_i}{c_j} \frac{(-1)^{i+j}}{(y_i - y_j)}, \quad i \neq j, \quad i, j = 1, \dots, N - 1, \\ c_i &= \begin{cases} 2, & i = 0 \text{ or } N, \\ 1 & \text{otherwise.} \end{cases} \end{aligned} \quad (9)$$

Derivation of the entries of the Chebyshev differentiation matrix are given in <https://micronanopi.net/newSUKIMA/Chebyshev/CDM/DerivationCDMinB.pdf>. The second derivative of ψ can be calculated by the product of D_N , so that $\psi'' = D_N(D_N \psi) = D_N^2 \psi$.

3.2 Discretization of the O-S equation and generalized eigenvalue problem

Confirming the validity of the CDM for drawing neutral stability curves is one of the objectives of this section. Non-dimension Poiseuille flow $\bar{U}(\bar{y})$ is expressed by

the equation $\bar{U} = 1 - \bar{y}^2$, and the flow is restricted to an interval $-1 \leq \bar{y} \leq 1$. The interval will be discretized by the following GCL points

$$\bar{y}_j = \cos \frac{j\pi}{N}, \quad j = 0, 1, \dots, N \quad (10)$$

The O-S equation can also be expressed by

$$i\alpha [(\bar{U} - c)(\phi'' - \alpha^2\phi) - \bar{U}''\phi] = \frac{1}{R}(\phi^{(4)} - 2\alpha^2\phi'' + \alpha^4\phi). \quad (11)$$

With the above discretization of the interval, $\phi(\bar{y})$ is rewritten with the column vector $(\phi_0, \phi_1, \dots, \phi_N)^T$. Transposition of the terms containing the complex velocity c to the right hand side in the above-mentioned O-S equation, and collect the terms not included in the left hand side, and then using the D_N we obtain

$$\left[\frac{1}{R}(D_N^4 - 2\alpha^2 D_N^2 + \alpha^4 \mathbf{I}) - i\alpha \bar{U}(D_N^2 - \alpha^2 \mathbf{I}) + i\alpha \bar{U}'' \mathbf{I} \right] \phi = -i\alpha c(D_N^2 - \alpha^2 \mathbf{I})\phi \quad (12)$$

Here \mathbf{I} is the identity matrix. Both sides of this equation are already a product of the $(N+1, N+1)$ matrix and the column vector of the $N+1$ component. Therefore $(N+1, N+1)$ matrices A and B are defined by

$$\left. \begin{aligned} A &\equiv \left[\frac{1}{R}(D_N^4 - 2\alpha^2 D_N^2 + \alpha^4 \mathbf{I}) - i\alpha \bar{U}(D_N^2 - \alpha^2 \mathbf{I}) + i\alpha \bar{U}'' \mathbf{I} \right], \\ B &\equiv -i\alpha(D_N^2 - \alpha^2 \mathbf{I}) \end{aligned} \right\}, \quad (13)$$

then the O-S equation (12) will be written by

$$A\phi = cB\phi.$$

From the above equation, the problem related to the O-S equation can be reduced to a generalized eigenvalue problem with c as its eigenvalue:

$$A = cB. \quad (14)$$

In the case of Rayleigh equation problem, from (7), matrices A and B are defined by

$$\left. \begin{aligned} \hat{A} &\equiv \bar{U}(D_N^2 - \alpha^2 \mathbf{I}) - \bar{U}'' \mathbf{I}, \\ \hat{B} &\equiv D_N^2 - \alpha^2 \mathbf{I} \end{aligned} \right\} \quad (15)$$

respectively. We use Scilab solver function “spec(A,B)” to solve the generalized eigenvalue problems numerically. We use the method Trefethen [3] calls “a simple trick”, that is $\phi(\bar{y})$ is replaced by

$$\phi(\bar{y}) = (1 - \bar{y}^2)q(\bar{y}). \quad (16)$$

From this replacement, $d^4\phi/d\bar{y}^4$ turns out to be

$$\frac{d^4\phi}{d\bar{y}^4} = (1 - \bar{y}^2) \frac{d^4q}{d\bar{y}^4} - 8\bar{y} \frac{d^3q}{d\bar{y}^3} - 12 \frac{d^2q}{d\bar{y}^2} \equiv \hat{D}^4 q(\bar{y}), \quad (17)$$

and also we get

$$\phi'(\bar{y}) = (1 - \bar{y}^2)q'(\bar{y}) - 2\bar{y}q(\bar{y}), \quad (18)$$

so that if $q(\pm 1) = 0$, then $\phi'(\pm 1) = 0$. When coding, $q(y) = \phi(y)/(1 - y^2)$ is written as $q(y) = S(y)\phi(y)$ by introducing $S(y) = 1/(1 - y^2)$. It should be noted that $S(\pm 1) = 0$ is assumed. Given a vector consisting of the value of the unknown function $q(\bar{y})$ at the GCL points as \mathbf{Q} , $q(\bar{y})$ is expressed by ϕ_i and $(N + 1, N + 1)$ matrix S as follows

$$Q_i = \frac{\phi_i}{1 - \bar{y}_i^2} = S_{ij}\phi_j, \quad S_{ij} = \frac{1}{1 - \bar{y}_i^2}\delta_{ij}. \quad (19)$$

(here δ_{ij} is Kronecker's δ). Therefore

$$\hat{D}^4\mathbf{Q} = \hat{D}^4S\phi, \quad (20)$$

then we obtain the matrix-type O-S equation

$$\left[\frac{1}{R}(\hat{D}^4S - 2\alpha^2D^2 + \alpha^4\mathbf{I}) - 2i\alpha\mathbf{I} - i\alpha(1 - \bar{y}^2)\mathbf{I}(D^2 - \alpha^2\mathbf{I}) \right] \phi = c \left[-i\alpha(D^2 - \alpha^2\mathbf{I}) \right] \phi. \quad (21)$$

Where we use the symbol $D_N^i \equiv D^i$. As described in Trefethen[3], in case of D^2 , the same operation for \hat{D}^4 is not done.

The matrices A and B are $(N + 1, N + 1)$ matrices, but since they are $\phi(\pm 1) = 0$ from the boundary condition, we drop the first and $N + 1$ columns of A and B . There are $N + 1$ equations whereas the unknowns are $N - 1$, so we drop the first row and the N row. Thus, matrices A and B are reduced to $(N - 1, N - 1)$ matrices. Details of Trefethen's method such as reduction of matrices etc. are described in Trefethen [3] chapters 7, 13, and 14.

3.3 Numerical results and neutral stability curves for Poiseuille flow

Following the work of Thomas (1953), Orszag[6], Dongarra et al, [7], eigenvalues were calculated as benchmark tests for $R = 10000$, $\alpha = 1$. The table 1 is the result: In this calculation we adopt $N = 200$.

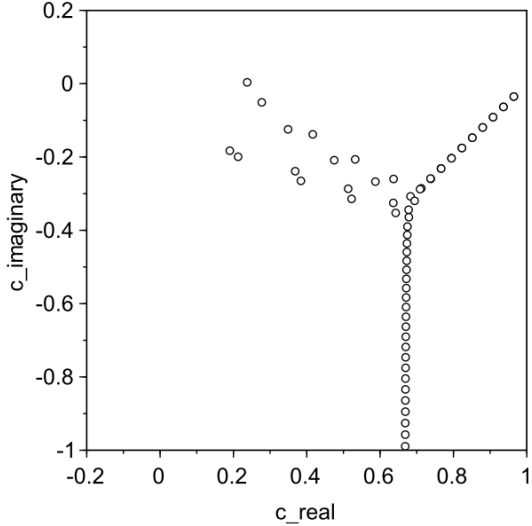
Table 1: Numerical results of eigenvalue

Thomas	$c = 0.23750060 + 0.00359250i$
Orszag	$c = 0.23752649 + 0.00373967i$
Dongarra et al.	$c = 0.23752708 + 0.00373980i$
Presented work	$c = 0.23752666 + 0.00373946i$

In Fig.1, a distribution of eigenvalues for the above case. The horizontal axis is the real part of the eigenvalue c and the vertical axis is the imaginary part. According to past studies, the critical Reynolds number of the plane Poiseuille flow was 5300 and $\alpha = 1.02$, but Orszag[6] was supposed to have the critical Reynolds number R_c and the critical α_c are as follows:

$$R_c = 5772.22, \quad \alpha_c = 1.02056 \pm 0.00001$$

In this case we represent the eigenvalues obtained by Orszag and the results in this paper in the table 2 ($N = 200$ in Scilab numerical simulation).

Figure 1: Distribution of eigenvalues for $R = 10000, \alpha = 1.0, N = 200$ Table 2: Critical Reynolds number and its eigenvalue ($\alpha = 1.02056$)

$R = 5772.22$	
Orszag	$c = 0.26400174 - 1.7 \times 10^{-9}i$
Presented work	$c = 0.26400148 - 9.6 \times 10^{-9}i$
$R = 5772.23$	
Orszag	$c = 0.26400166 + 1.3 \times 10^{-8}i$
Presented work	$c = 0.26400166 + 2.2 \times 10^{-8}i$

Perform the following procedure to find a neutral stability curve. First fix α_0 and increase Reynolds number R by just 1 from a certain value R_{init} (integer). At this time, eigenvalues for each R are found, and R_0 where the sign of the imaginary part changes is searched and this point is set as (R_0, α_0) . Next increase α such that $\alpha_1 = \alpha_0 + h_\alpha$. Now fixed the α_1 , then increase R again by 1 from a certain value R_{init} , find the Reynolds number R_1 at which the sign of the imaginary part of the eigenvalue varies, and set (R_1, α_1) . Repeat this to find a neutral stability curve. We set $h_\alpha = 0.05$ in interval $0.1 \leq \alpha \leq 1.0$, $h_\alpha = 0.01$ in interval $1.01 \leq \alpha \leq 1.09$, $h_\alpha = 0.001$ in interval $1.091 \leq \alpha \leq 1.094$, and found a neutral stability curve, which is shown in Figure 2.

In the figure, the horizontal axis is the Reynolds number and the vertical axis is the value of α . The figure 3 is an enlargement of kink on the upper asymptotic branch, but it is characteristic that the slope of the first half curve from the minimum to the maximum is negative (: R decreases in the interval of $0.327 \leq \alpha \leq 0.340$)¹.

¹In Figure2, the Reynolds number is shown up to $R = 1.0 \times 10^9$, but in the unstable

The minimal and maximal coordinates each appear in the following coordinates:

$$(R, \alpha) = (107520000 \pm 2430000, 0.326498), \\ (R, \alpha) = (114990000 \pm 40000, 0.343330).$$

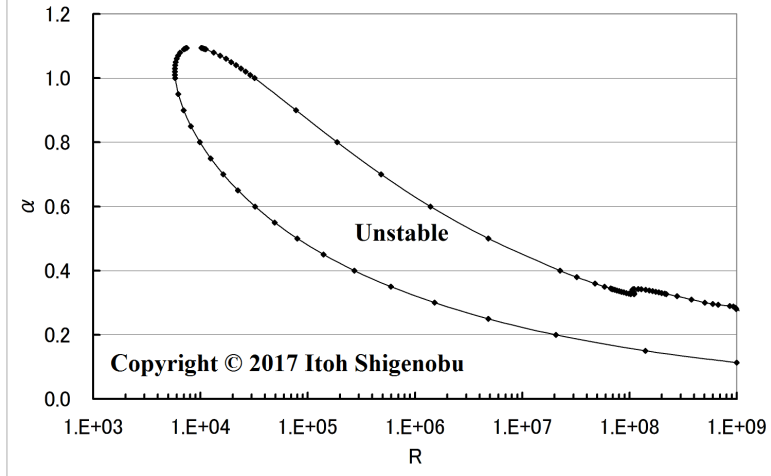


Figure 2: A neutral stability curve for Poiseuille flow

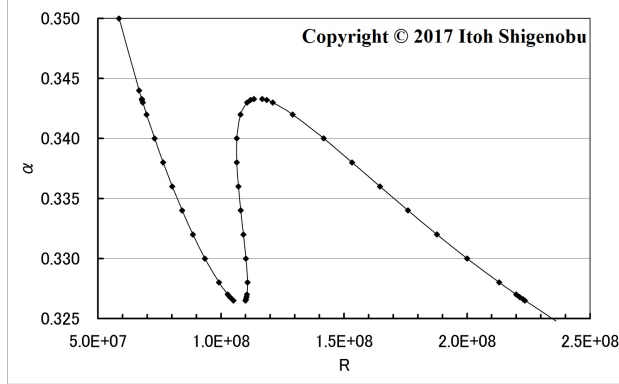


Figure 3: An enlargement of kink on the upper branch

Figure 4 shows the behavior of the imaginary part c_i on the cross-section where the Reynolds number is constant on the (R, α) plane of figure 2(that is, the behavior of c_i of eigenvalues $c = c_r + c_i i$ when Reynolds number R is constant and α is changed). Here, the numerical value such as $5.E + 07$ attached to the curve is the value of the Reynolds number.

region of $R > 2.52 \times 10^9$, a stable region occurs in a shape like a cavity. A.G.Walton [8] points out that similar cavity occurs in the Poiseuille flow in the pipe.

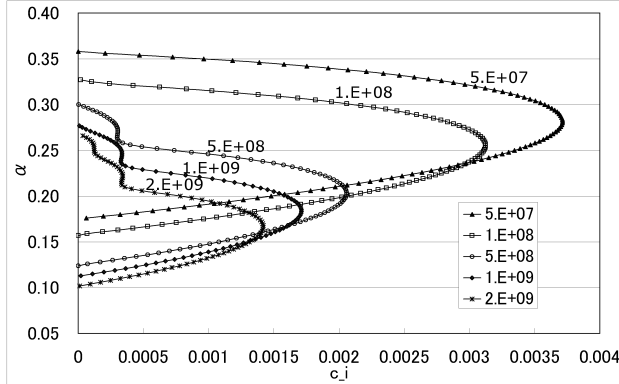


Figure 4: The behavior of the imaginary part of eigenvalues for each Reynolds number R . Horizontal c_i , Vertical α

4 Neutral stability curve for the laminar boundary layer

4.1 Nondimensionalization in the y -axis direction and dimensionless quantity

In the case of boundary layer flow, the alternative length to the characteristic length \mathcal{L} is $\delta(x)$ which is defined by the following expression:

$$\delta(x) = \sqrt{\frac{\nu x}{U_0}}, \quad (22)$$

where U_0 is the main flow velocity at infinity and x is the distance from the leading edge of the boundary layer. The length y in the y -axis direction becomes dimensionless as $\bar{y} = y/\delta(x)$ by the above length. The Reynolds number appearing in the

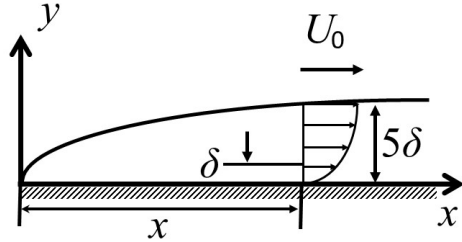


Figure 5: Boundary layer flow : U_0 is the main flow speed at infinity.

O-S equation (5) is also assumed here as $R = U_0\delta(x)/\nu$.

4.2 Semi-infinite region and CDM

The \bar{y} axis area of the boundary layer flow is $0 \leq \bar{y} < \infty$. Therefore, in order to allocate the GCL point, this semi-infinite region must be mapped to the finite region. Several mapping functions are conceivable, but here we refer to Theofilis[9].

$$\bar{y} = L \frac{1 - \eta}{3 + \eta} \quad (23)$$

Here, the region where the GCL point is taken is represented as η and taken as $-1 \leq \eta \leq 1$. Theofilis cite Theofilis has chosen the value $L = 50$. $\eta = 1$ and $\bar{y} = 0$ (on the flat plate), while $\eta = -1$ and $\bar{y} = 50$, so it will not be infinity. However, in the case of the laminar boundary layer, since the velocity reaches the infinite speed at the point where the dimensionless \bar{y} is about 5, the value $L = 50$ can be considered far enough.

For example, if $\bar{y} = (1 - \eta)/(1 + \eta)$ is used as the mapping function, $\bar{y} = \infty$ at $\eta = -1$ so that infinity as a distance is achieved. But infinity as magnitude occurs.

The relationship between $d/d\bar{y}$ and $d/d\eta$ by using the mapping function (23) is as follows. To simplify the notation, $\zeta \equiv 3 + \eta$, $\ell \equiv 4L$, $(d/d\eta)^i \equiv \mathcal{D}^i$ as follows:

$$\begin{aligned} \frac{d}{d\bar{y}} &= -\frac{\zeta^2}{\ell} \frac{d}{d\eta} = -\frac{\zeta^2}{\ell} \mathcal{D}, \\ \frac{d^2}{d\bar{y}^2} &= \frac{1}{\ell^2} (2\zeta^3 \mathcal{D} + \zeta^4 \mathcal{D}^2), \\ \frac{d^3}{d\bar{y}^3} &= -\frac{1}{\ell^3} (6\zeta^4 \mathcal{D} + 6\zeta^5 \mathcal{D}^2 + \zeta^6 \mathcal{D}^3), \\ \frac{d^4}{d\bar{y}^4} &= \frac{1}{\ell^4} (24\zeta^5 \mathcal{D} + 36\zeta^6 \mathcal{D}^2 + 12\zeta^7 \mathcal{D}^3 + \zeta^8 \mathcal{D}^4), \end{aligned} \quad (24)$$

4.3 The O-S equation for the laminar boundary layer

Review the notation of dimensionless quantities for laminar boundary layer. Abbreviated as $\delta(x) = \delta$, and make dimensionless coordinates in the $y-$ axis direction as follows:

$$\bar{y} = \frac{y}{\delta} = y \sqrt{\frac{U_0}{\nu x}}. \quad (25)$$

The velocity $\mathbf{u} = (U, V)$ in the 2-dimensional boundary layer will be given by

$$U = U_0 f'(\bar{y}), \quad V = \frac{1}{2} \sqrt{\frac{\nu U_0}{x}} [\bar{y} f'(\bar{y}) - f(\bar{y})]. \quad (26)$$

And with using the function f , the laminar boundary layer equation is

$$2f''' + ff'' = 0, \quad ('' \equiv d^2/d\bar{y}^2 \text{ etc.,}) \quad (27)$$

(that is Blasius equation). Considering $U/U_0 \equiv \bar{U} = f'$, $\bar{U}'' = f'''$, the O-S equation becomes

$$i\alpha \left[(f' - c)(\phi'' - \alpha^2 \phi) - f''' \phi \right] = \frac{1}{R} (\phi^{(4)} - 2\alpha^2 \phi'' + \alpha^4 \phi). \quad (28)$$

where $R = U_0 \delta / \nu$.

4.4 The solution for Blasius equation

The O-S equation contains mainstream $\bar{U} = f'(\bar{y})$ and $\bar{U}'' = f'''(\bar{y})$. Therefore, the solution of the nonlinear third order differential equation (27) that represents the laminar boundary layer is necessary, but here it is obtained by the numerical solution method of the ordinary differential equations by the Shooting method mentioned which we refer it in the next section. So obtained solution is the same as the solution described in the reference[2]. Divide \bar{y} by the step width 0.2, and let the generated point be \bar{y}_i . We calculate f_i , f'_i and f''_i at these points \bar{y}_i , and further obtain their values at the GCL points by interpolation. In this case, the interpolation value was obtained by the iterative method of Aitken-Neville using 20 points. Hereinafter, this flow is called Blasius boundary layer.

4.5 Reduction to generalized eigenvalue problem

The method of discretizing the O-S equation (??) at the GCL points and making it into a matrix form is exactly the same as that of Poiseuille flow. However, as we have mapped from the infinite region to the bounded region (24), the derivative is complicated here.

One of the features of this numerical experiment is that a simple trick (24) by Trefethen[3] for D^4 in the equations (16) was applied. Also, as with Poiseuille flow, boundary conditions are being treated. When coding, for $\bar{U} = f'(\bar{y})$ and $\bar{U}'' = f'''(\bar{y})$, matrices having diagonal components equal to the number of GCL points are created, and interpolated values are given to each diagonal elements.

4.6 Comparison of numerical experiments for the Blasius boundary layer

In order to examine the setting value of infinity, we chose $L = 50, 100, 200, 500$ as L of the mapping function (23). Only $L = 50, N = 128$ is written in Theofilis[9], and this paper also adopted this case for comparison (Table3 Case I). In addition to 4 cases, we set 5 cases in total, and summarize those in Table 3. In the table, the numbers in parentheses are approximate numbers of GCL points taken in the boundary layer.

Table 3: Numerical experiments setting table

	$L = 50$	$L = 100$	$L = 200$	$L = 500$
$N = 128$	I (49)	*	*	*
$N = 256$	II (96)	III (68)	IV (49)	*
$N = 384$	*	*	*	V (48)

Comparison between our results and other articles for Case I

Comparison between our results and those by Theofilis[9], and Macaraeg et al.[10] for Case I is shown in Table4. As a result of the comparison in the table 4, the Scilab results almost coincide with the other two up to the fourth digit after the decimal

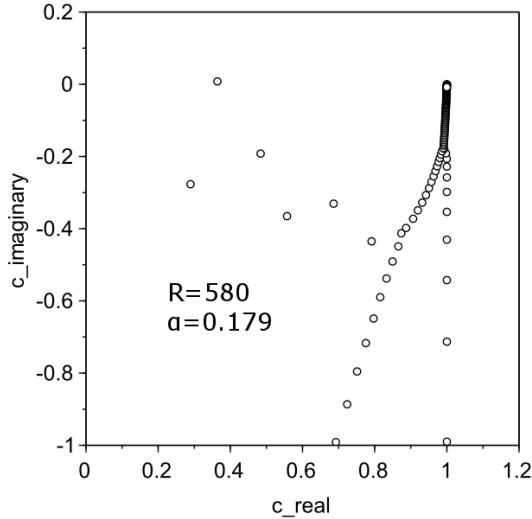


Figure 6: Distribution of eigenvalue for Case I

point for both the eigenvalue real and imaginary parts. Furthermore, the results of Scilab almost agree with Theofilis ($N = 128, L = 50$) up to the fifth decimal place. Also in the case I, the eigenvalue distribution when $\alpha = 0.179$, $R = 580$ is shown in the Figure 6.

4.7 A neutral stability curve for the laminar boundary layer

In the same way as in Poiseuille flow, a neutral stability curve was drawn, but here, like the other articles [2], the wavenumber on the vertical axis of the graph is dimensionless by the displacement thickness δ^* . Therefore, the horizontal axis Reynolds number is also set as $R^* = U_0\delta^*/\nu$ (Fig.7, Fig.8). The experimental values of Schubauer et al. were read from Figure 3.10.5 of "Flow stability theory" [1]. Also, the horizontal axis of the figure 8 enlarging the kink part is not a logarithmic scale.

Calculations are executed with $\alpha, R = U_0\delta/\nu$ as before. Therefore we get α by the equation $\alpha = \alpha^*/1.7208$. In Figure 7 we set $h_{\alpha^*} = 0.001$ for the curve vertex $0.345 \leq \alpha^* \leq 0.356$.

Around the kink, we choose $h_{\alpha^*} = 0.0001$, and some points near the kink are shown for some cases in Table 5. In Table 5, R is the Reynolds number defined by δ , so that R is integer. While non-dimensional wavenumber is the one by δ^* . As shown in Table 5, it is understood that kink occurs in all cases. As can be seen from the same table, the L dependency slightly appears in the location of the local maximum and minimum. However these curves approach in the vicinity of $\alpha^* = 0.13$ at the limit of $L \rightarrow 500$.

In the upper asymptotic branch, the case of I, II, III, IV, V coincides at each point of $0.18 \leq \alpha^* \leq 0.36^2$, in the section of $0.14 \leq \alpha^* \leq 0.36$, the curves of cases

²However, only for $\alpha^* = 0.18$, case I and case II are $R = 10756$, while in case III, IV

Table 4: Comparison between our results and other articles for Case I

$\alpha = 0.179, R = 580$	
Macaraeg	$c_1 = 0.3641 + 0.0080i$
	$c_2 = 0.2897 - 0.2769i$
	$c_3 = 0.4839 - 0.1921i$
	$c_4 = 0.5572 - 0.3653i$
	$c_5 = 0.6862 - 0.3307i$
Theofilis	$c_1 = \bar{0.3641} \bar{212880} + \bar{0.0079625034}i$
	$c_2 = 0.2897243201 - 0.2768738567i$
	$c_3 = 0.4839439094 - 0.1920824050i$
	$c_4 = 0.5572212338 - 0.3653515279i$
	$c_5 = 0.6862882375 - 0.3307860195i$
Case I	$c_1 = \bar{0.3641} \bar{229207} + \bar{0.0079597113}i$
	$c_2 = 0.2897144377 - 0.2768665293i$
	$c_3 = 0.4839294091 - 0.1920673182i$
	$c_4 = 0.5571929853 - 0.3653411623i$
	$c_5 = 0.6862869476 - 0.3307141089i$

III, IV and V become the same one³.

In the case of the lower branch, all cases are the same curve in the interval $0.14 \leq \alpha^* \leq 0.356$.⁴. As described above, in the case of the upper branch, in the interval $\alpha^* \gtrsim 0.13$, it is considered that the curve goes to convergence when $L \rightarrow 500$, but when $\alpha^* < 0.1$, the variation of the curve due to the value of L is large. Also in the case of the lower branch, the curve varies depending on the value of L in the $\alpha^* < 0.08$. The value of N has to be increased by increasing L , so the problem of PC performance also. As in the case of Poiseuille flow, the behavior of the imaginary part of the eigenvalue when α is continuously changed as Reynolds number $R^* = \text{constant}$ near kink is shown in Fig.9.

4.8 Critical Reynolds number R_{criti}^* for the boundary layer

According to the stability theory of the 1940's, the critical Reynolds number R_{criti}^* of the boundary layer flow was assumed to be

$$R_{\text{criti}}^* = \left(\frac{U_0 \delta^*}{\nu} \right)_{\text{criti}} = 420 \quad (29)$$

also $\alpha^* = 0.34$ (Lin(1945)⁵). Judging from the graph of neutral stability curve by Scilab simulation presented here, $\alpha^* = 0.3$ is considered to be critical, at that

and case V $R = 10759$. Where $R = U_0 \delta / \nu$.

³Only for $\alpha^* = 0.14$ is $R = 28750$ in case III and $R = 28752$ in other cases.

⁴Only in case of $\alpha^* = 0.14$, $R = 856$ in cases I and II, and $R = 857$ in case III, IV and V.

⁵http://thesis.library.caltech.edu/2696/1/Lin_cc_1944.pdf.

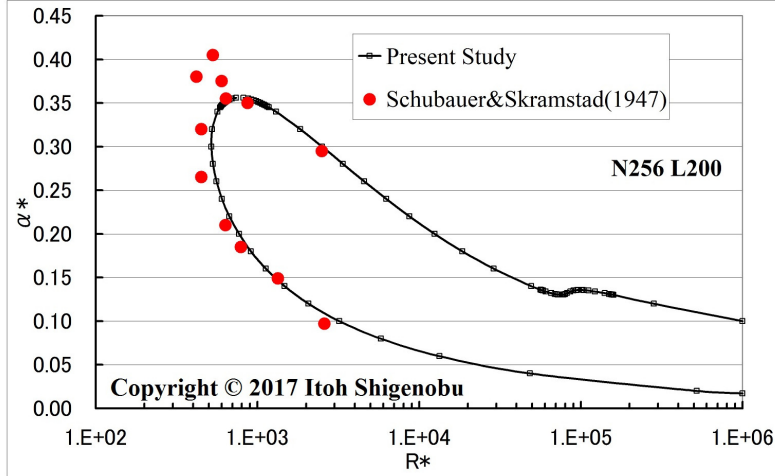


Figure 7: A neutral stability curve for the laminar boundary layer

time $R_{\text{criti}}^* = 517.7$, which is close to Jordinson's 520. Note that this value is the same for all cases I to V (from the coincidence of lower branches)⁶.

5 A neutral stability curve of the Falkner-Skan boundary-layer flow

5.1 Falkner-Skan equation

The Falkner-Skan equation is an equation representing the boundary layer flow in the presence of a pressure gradient in the outer stream of the boundary layer and is given by

$$f''' + \beta_0 f f'' + \beta(1 - f'^2) = 0 \quad (30)$$

where $\beta \neq 0$, in general. That is, if the x -direction velocity component of the flow in the boundary layer is $u(x)$ and the x -direction velocity component of the flow outside the boundary layer is $U_e(x)$, it is defined as $f' = u/U_e$. The details of the derivation of Equation (30) are given in Chapter 8 of Schlichting[2]. As long as $\beta_0 \neq 0$, its value can be arbitrarily set, and $\beta_0 = 1$ below. Also, the dimensionless coordinates corresponding to (25) and the characteristic length δ are defined as follows

$$\bar{y} = \frac{y}{\delta} : \quad \delta = \sqrt{(2 - \beta) \frac{\nu x}{U_e}} \quad (31)$$

The derivative symbol ('') is the same as in section 4 ($f' = df/d\bar{y}$). The boundary conditions are

$$f(0) = 0, \quad f'(0) = 0, \quad \text{for } \bar{y} = 0, \quad f' \rightarrow 1 \quad \text{for } \bar{y} \rightarrow \infty. \quad (32)$$

⁶More precisely, $\alpha^* = 0.3035 \pm 0.0045$ and $R_{\text{criti}}^* = 517.7$.

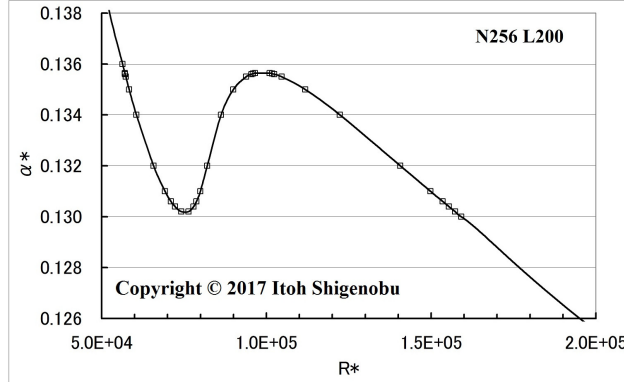


Figure 8: An enlargement around the kink on the neutral stability curve of the boundary-layer.

In the case of $\beta \geq 0$, the velocity profile does not have inflection points, whereas in the case of $-0.1988 \leq \beta < 0$, its velocity profile has inflection points. Here, the minimum value $\beta = -0.1988$ corresponds to the case where separation of flow appears. The velocity profile for several β discussed here is shown in Fig.10.

The horizontal axis is the dimensionless speed f' and the vertical axis is the direction \bar{y} perpendicular to the flat plate defined by (31). The values and symbols of β are shown in the legend in Figure 10, but the order in this legend and the order of velocity profile in the figure correspond from the top to the bottom.

5.2 On the numerical solution of the Falkner-Skan equation with Shooting method

In the shooting method, $f''(0) = s$ is added to the boundary condition (32), so that the boundary condition is changed with for $\bar{y} = 0$, $f(0) = f'(0) = 0$, $f''(0) = s$. Here, s is an arbitrary unknown value. Then give a value to s and solve the Falkner-Skan equation under the new boundary condition. Furthermore, we adjust the value of s and search for a solution where $f \rightarrow 1$ for $y = \infty$. This method is called Shooting method. For the integration, Scilab solver Runge-Kutta 4 is used. In order to compare with the results published by Asaithambi [12] we selected beta same as them and calculated for it. For each β , the value of $f''(0) = s$ for the flow solution is displayed in Table 6. A solution of Falkner-Skan flow for each β was obtained by Shooting method with \bar{y} as 0.2 step width. As in the previous section, the values of f' , f''' on $\bar{y}_i = 0.2 * i$, ($i = 0, 1, 2, \dots$) were interpolated on the GCL points.

5.3 Displacement thickness δ^* for each β

In the previous section, we used the displacement thickness δ^* , which is one of the parameters indicating the thickness of the boundary layer, in the neutral stability curve of the boundary layer, but here again we define this displacement

Table 5: Non-dimensional wavenumber α^* and Reynolds number R near the kink on the upper branch

Case	α^*	R_0	R_1	R_2
Case I $N = 128$, $L = 50$	0.1360	32603	--	--
	0.1355	33168	56326	58586
	0.1350	33756	52837	63974
	0.1300	43160	44443	91545
	0.1280	--	--	102822
	0.1360	32733	--	--
Case IV $N = 256$, $L = 200$	0.1355	33308	54522	60798
	0.1350	33905	52261	64976
	0.1302	43088	44377	91380
	0.1300	--	--	92482
	0.1360	32733	--	--
	0.1355	33308	54472	60889
Case V $N = 384$	0.1350	33905	52243	65022
	0.1302	43093	44369	91166
	0.1300	--	--	92260
	0.1360	32733	--	--

thickness:

$$\begin{aligned} \delta^* &= \sqrt{(2 - \beta) \frac{\nu x}{U_e}} \int_0^\infty (1 - f'(\bar{y})) d\bar{y} \\ &\equiv \Delta \sqrt{(2 - \beta) \frac{\nu x}{U_e}}. \end{aligned} \quad (33)$$

As the boundary layer flow also changes with the change of β , the displacement thickness also changes correspondingly. Therefore, here, we preliminarily calculate the coefficient Δ related to displacement thickness for each β (Table 7). The coefficient *Theta*⁷ of momentum thickness θ which is not directly related to this discussion is also listed in the table for verification. Furthermore we also noted y that $f' = 0.9990$ (see Wazzan et al. [5]). In the calculation of \bar{y}_δ , the step size of \bar{y} is set to 0.01.

5.4 Neutral stability curves for Falkner-Skan boundary-layer

The method for finding a neutral stability curve for this problem is exactly the same as in the previous section. The eigenvalue distributions obtained from the O-S equation for the flow of 3 cases with $\beta = 1.6, 0.0 - 0.1988$ are shown (Figs.11,12,13). In each case $\alpha^* = 0.1, R^* = U_e \delta^* / \nu = 1000$.

⁷the momentum thickness θ and its coefficient Θ

$$\theta = \sqrt{(2 - \beta) \frac{\nu x}{U_e}} \int_0^\infty f'(1 - f') d\bar{y} \equiv \Theta \sqrt{(2 - \beta) \frac{\nu x}{U_e}}$$

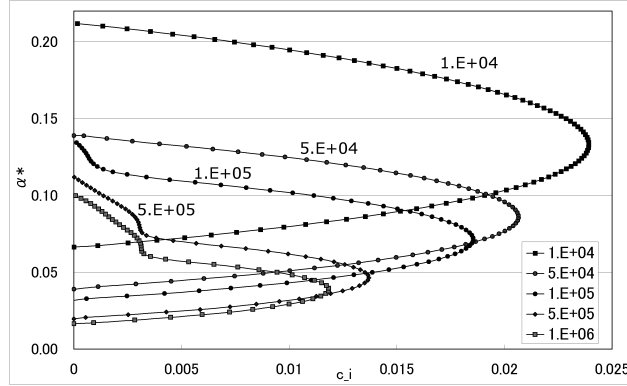


Figure 9: The behavior of the imaginary part of eigenvalues for each Reynolds number R . Horizontal c_i , Vertical α^*

Table 6: Comparison of results of Shooting method

β	Presented $f''(0)$	Asaithambif''(0)
1.0	1.232594	1.232589
0.5	0.927680	0.927680
0.0	0.469601	0.469600
-0.1	0.319270	0.319270
-0.15	0.216361	0.216361
-0.18	0.128642	0.128637
-0.1988	0.005232	0.005225

5.4.1 Case for $\beta > 0$

When $\beta > 0$ in equation (30), the velocity profile of the flow in the boundary layer is a convex flow in the downstream direction (Figure 10). As β increases, the neutral stability curve initially moves its vertex downwards ($0 \lesssim \beta \lesssim 0.6$). In the case of $\beta = 0.05, 0.1, 0.3, 0.6$, kink on the upper asymptotic branch seems to be moving below $\alpha^* = 0.05$, we could not catch numerically. However, we can catch kink again by increasing β . When β is increased from 0.6, the upper asymptotic branch newly bulges upward. The neutral stability curve for $\beta = 1.6$ is shown in Figure 17 again. As in the case of the Blasius boundary layer, the behavior of the imaginary part c_i of eigenvalues in the five cross-sections of Fig.17 is shown in Fig. 18.

5.4.2 Case for $\beta = 0$

If $\beta = 0$ in the equation (30), the flow corresponds to the boundary layer flow on the flat plate. However, since $\beta_0 = 1$, it is numerically different from the Blasius boundary layer flow in the previous section. Here, we also showed the neutral stability curve when β was changed to positive and negative by 0.01, and the

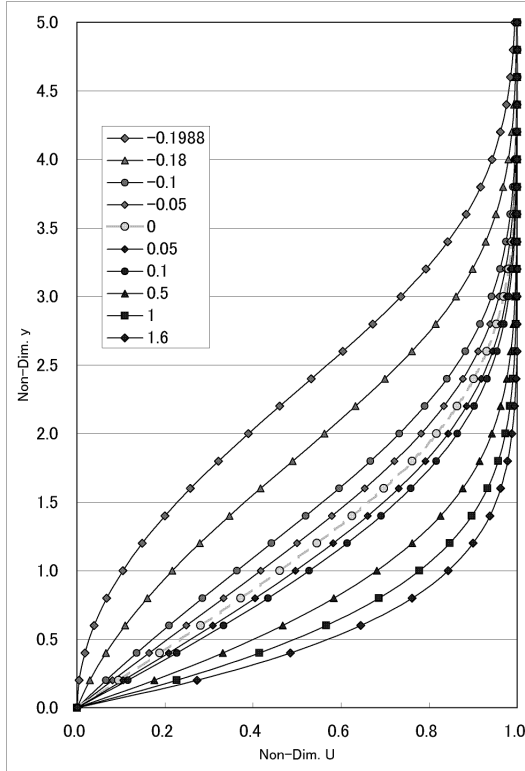


Figure 10: The velocity profile of the Falkner-Skan flow

change was illustrated (Fig. 19).

To change β from zero to positive corresponds to the case where the flow pressure outside the boundary layer decreases towards the downstream, the flow in the boundary layer accelerates. In this case, since the eigenvalue search where the imaginary part of the eigenvalue is zero could not be extended to $R^* = 1.0 \times 10^6$, the maximum Reynolds number R^* was set to 5.0×10^5

5.4.3 Case for $\beta < 0$

This case is when there is an inflection point in the velocity profile. Figure 21 shows the result of calculating the neutral stability curve as before. As represented by $\beta = -0.1988$, the curve has two branches, that is, $\alpha^* \rightarrow 0$ and $\alpha^* \rightarrow \text{const.}$ at the limit of the Reynolds number $R \rightarrow \infty$. The upper limit of the upper asymptotic branch of the curve in Figure 21 coincides with the value in the chart of Wazzan et al. at $R^* = 1.0 \times 10^5$ (the maximum value of the Reynolds number R^* of Wazzan et al. is 1.0×10^5). In the chart of Wazzan et al., a kink on the upper branch is not captured. The upper limit of the upper branch of the curve in Figure 21 coincides with the value in the chart of Wazzan et al. on $R^* = 1.0 \times 10^5$ (the maximum value of the Reynolds number R^* of Wazzan et al. is 1.0×10^5). In the chart of Wazzan et

Table 7: Coefficient of displacement thickness and others for each β

β	Δ	Θ	\bar{y}_δ
1.60	0.5417	0.2481	2.63
1.00	0.6479	0.2923	3.14
0.80	0.6987	0.3118	3.28
0.60	0.7640	0.3359	3.44
0.30	0.9110	0.3858	3.75
0.10	1.0803	0.4355	4.05
0.05	1.1417	0.4515	4.14
0.03	1.1698	0.4584	4.19
0.02	1.1848	0.4621	4.21
0.01	1.2004	0.4658	4.23
0.00	1.2168	0.4696	4.26
-0.01	1.2340	0.4735	4.28
-0.05	1.3124	0.4905	4.39
-0.1	1.4427	0.5151	4.56
-0.14	1.5959	0.5386	4.75
-0.18	1.8716	0.5677	5.06
-0.1988	2.3330	0.5854	5.54

al., kink on the upper branch is not captured. The enlargement around the kink is shown in Figure 22. The behavior of the imaginary part c_i on the neutral stability curve of $\beta = -0.1988$ on the Reynolds number constant cross section is shown in Figure 23.

Rayleigh equation

Rayleigh succeeded in deriving several important theorems concerning the stability of laminar velocity profiles. The first important ‘general theorem’ of this kind, so-called, *point – of – inflexion criterion*, asserts that velocity profiles which possess a point of inflexion are unstable. (see [2]p.445). In the case of $\beta < 0$, there are two intervals where $\bar{U}'' > 0$ and $\bar{U}'' < 0$ in the region $0 \leq \bar{y} < \infty$, and its inflection point is represented by \bar{y}_s : $\bar{U}''(\bar{y}_s) = 0$.

In the case of $\beta < 0$, we obtain eigenvalues such that $c_i > 0$ for a certain range of dimensionless wavenumber α^* ⁸. The eigenvalue distribution by the Rayleigh equation when $\beta = -0.1988, \alpha^* = 0.1$ is shown in Figure 24. For comparison, the eigenvalue distribution obtained from the O-S equation for $R^* = 1.0 \times 10^6, \alpha^* = 0.1$ is shown in Figure 25. The eigenvalue (: complex conjugate) for $c_i \neq 0$ in Figure 24 is

$$0.13308694 \pm 0.13391664i,$$

⁸When we denote the velocity at the inflection point by $\bar{U}_s = \bar{U}(y_s)$, we obtain $\bar{U}''(\bar{U} - \bar{U}_s) < 0$ for the flow dealt with here. This is the case where the condition in Fjørtoft’s theorem holds.

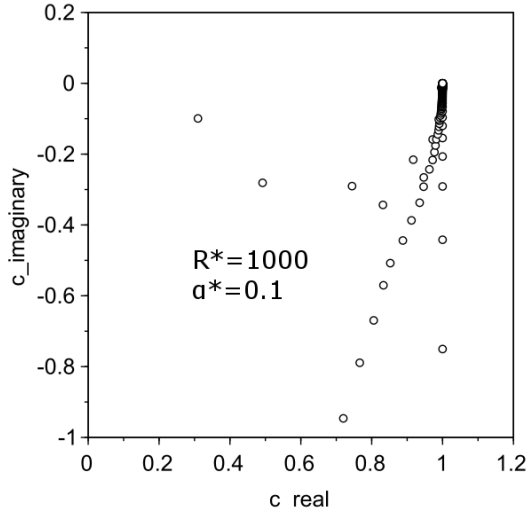


Figure 11: Eigenvalue distribution of O-S equation for $\beta = 1.6$

while in Figure 25 those are

$$0.13403886 + 0.13251756i, \\ 0.13170933 - 0.13296710i.$$

Furthermore, the behavior of the imaginary part of the eigenvalue calculated by the Rayleigh equation in the case of $\beta = -0.1988, -0.18, -0.14, 0.1$ is shown in Figure 26.

6 Conclusion

Numerical experiments using Scilab were conducted and the following results were obtained:

- (1) Using the Chebyshev Differentiation Matrix related to the spectral method, we reduced the Orr - Sommerfeld equation problem to a generalized eigenvalue problem and found a neutral stability curve of Poiseuille flow. Local minimum and maximum (: kink) appears in the upper branch of the curve near Reynolds number $R = 1.0 \times 10^8$.
- (2) As in the above (1), a neutral stability curve for Blasius boundary layer flow was obtained. The curve is in good agreement with the experiments of Scubauer and Skramstad at nine points except three points with large wavenumbers. Similarly to the Poiseuille flow kink appears around the upper branch of the curve $R^* = 1.0 \times 10^5$.
- (3) The critical Reynolds number R_{criti}^* in Blasius boundary layer is 517.7.
- (4) The parameter β of the Falkner-Skan equation (30) was changed to positive, zero and negative to obtain a neutral stability curve for the flow in each case. As a result, it was confirmed that kink occurred in the upper branch of the curve regardless of the sign of β .
- (5) As a result of applying a flow having an inflection point to the velocity profile

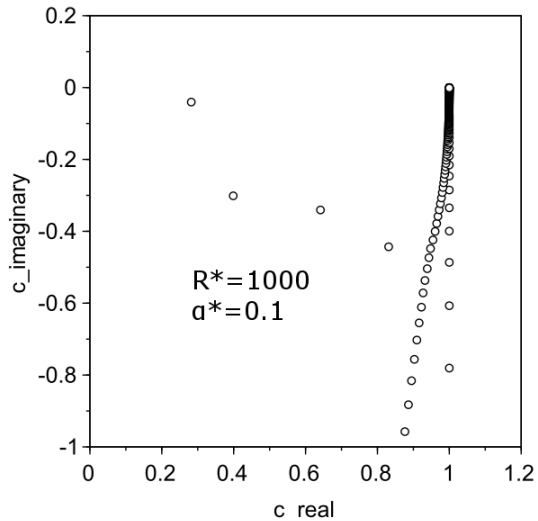
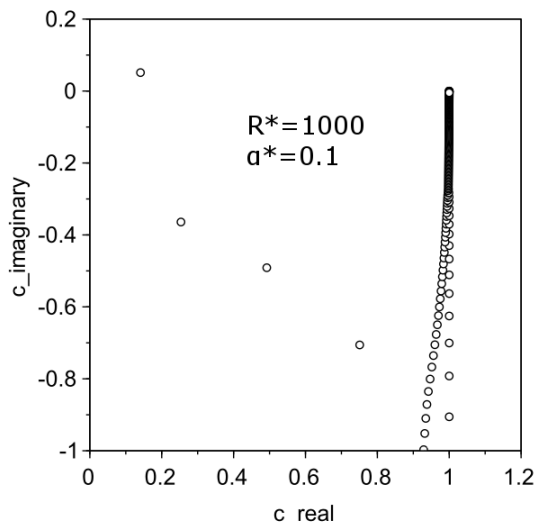
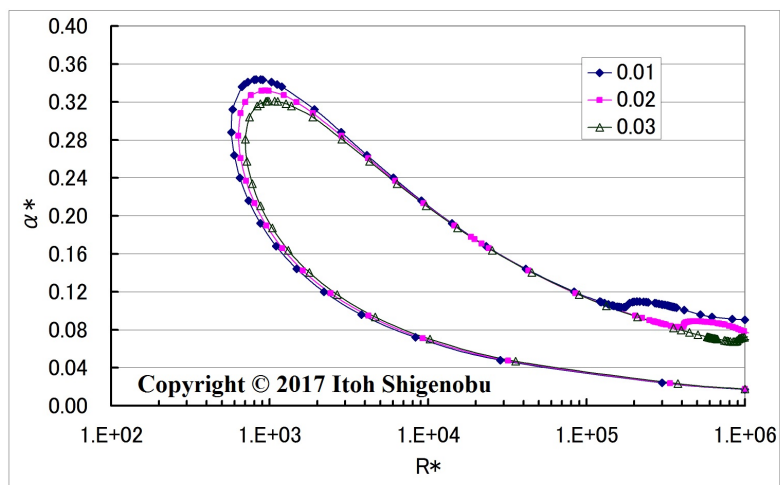
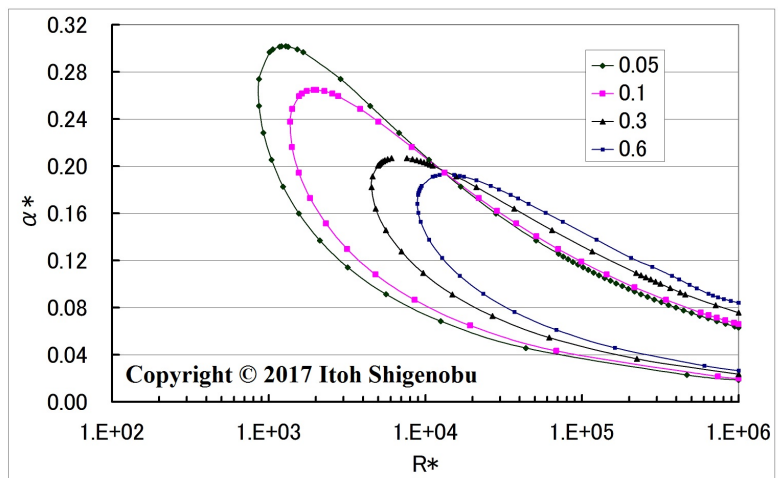
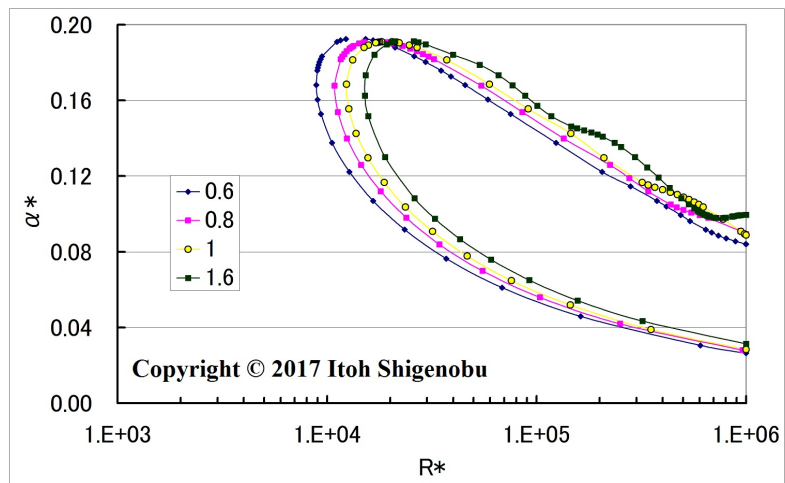


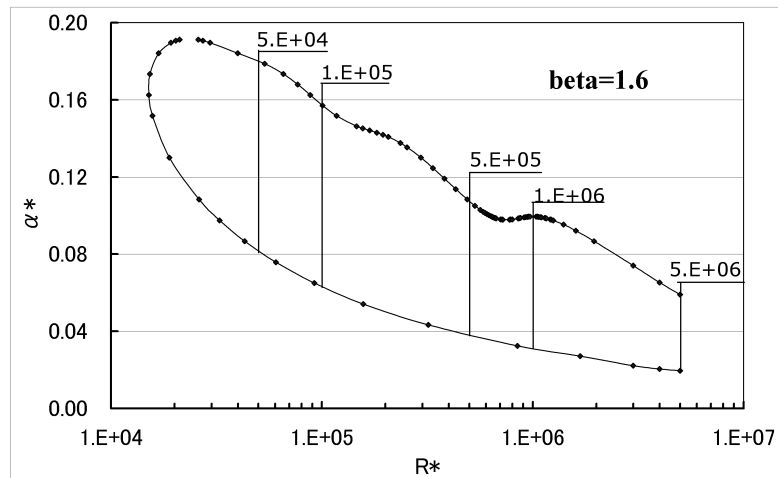
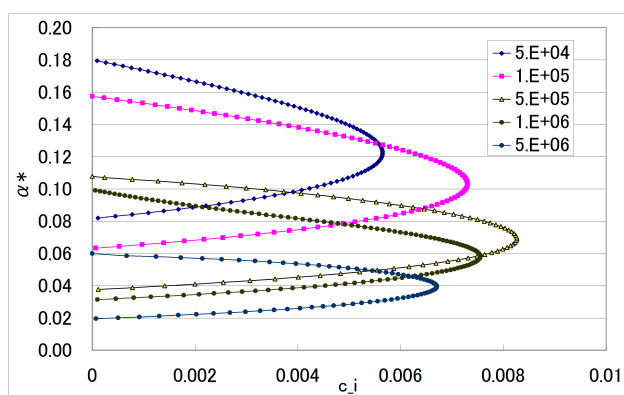
Figure 12: Eigenvalue distribution of O-S equation for $\beta = 0.0$

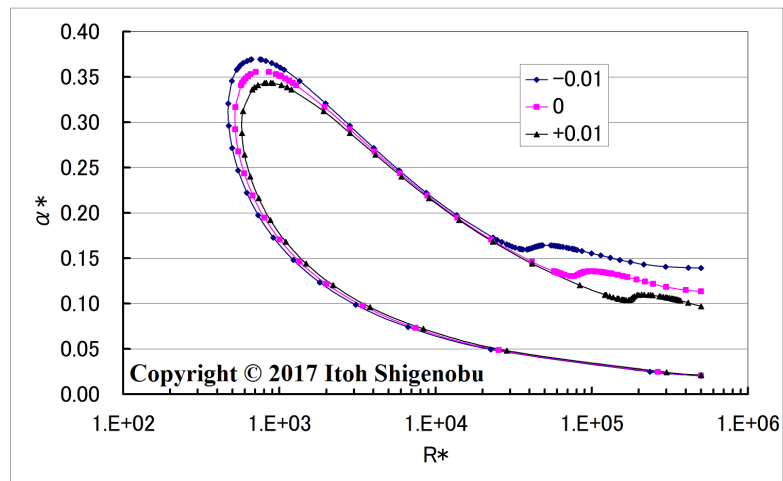
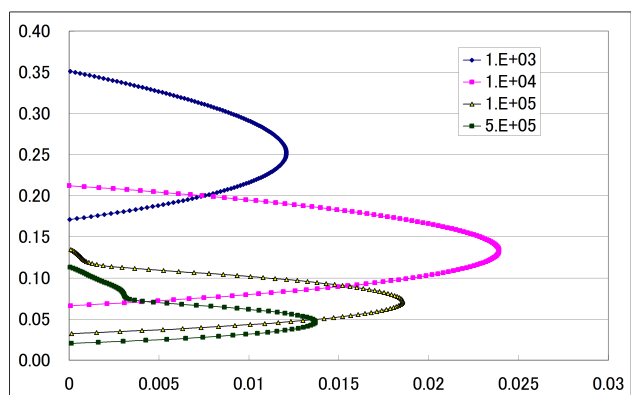
to the Rayleigh equation, it was confirmed that an eigenvalue exists in which the imaginary part of the eigenvalue is positive ($:c_i > 0$).

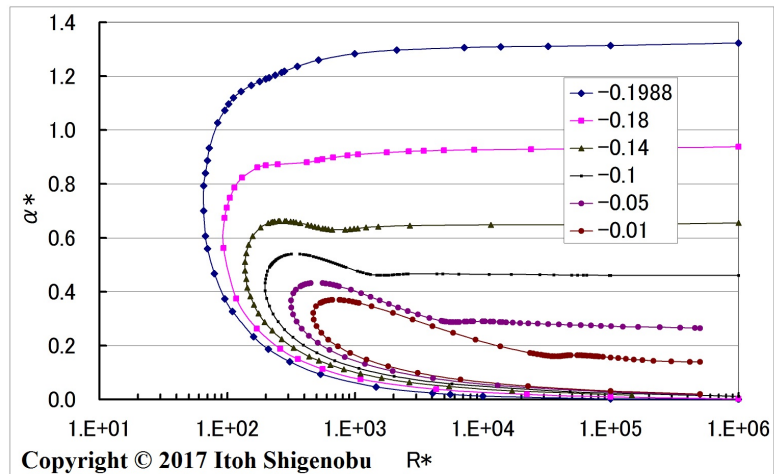
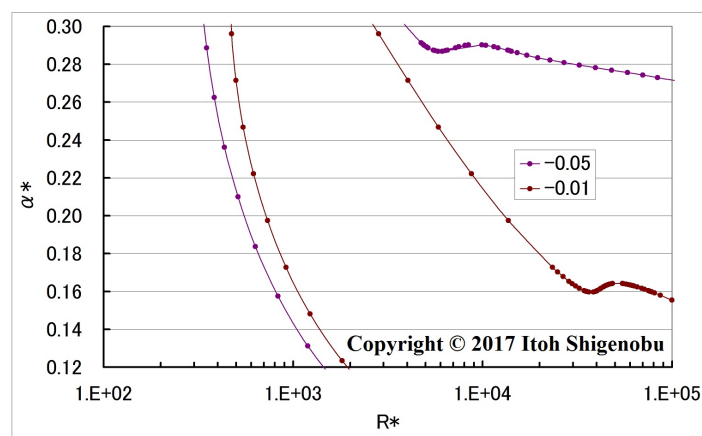
(6) From the above results of (1), (2) and (4), it was confirmed that local minimum and maximum (:kink) appears on the upper branch of neutral stability curves of various flows.

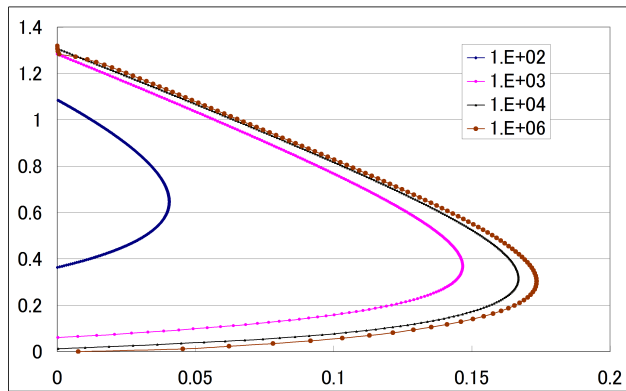
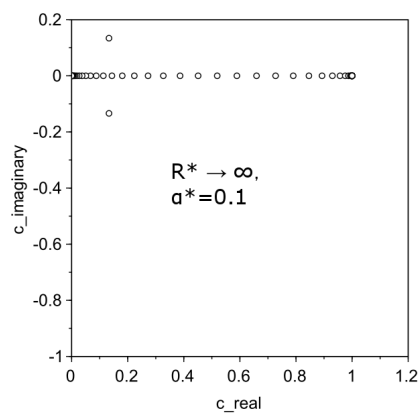
Figure 13: Eigenvalue distribution of O-S equation for $\beta = -0.1988$ Figure 14: Neutral stability curves for $\beta = 0.01, 0.02, 0.03$

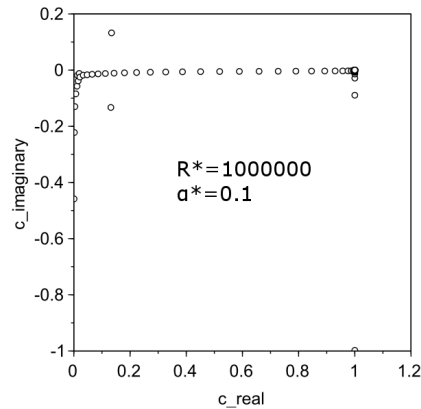
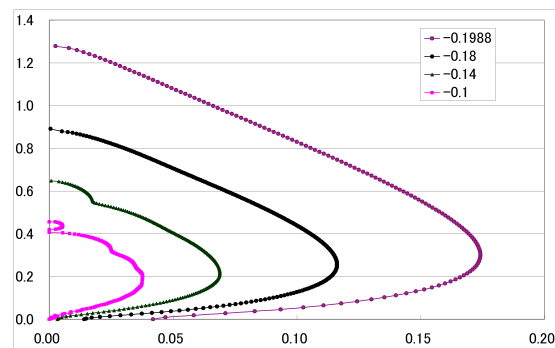
Figure 15: Neutral stability curves for $\beta = 0.05, 0.1, 0.3, 0.6$ Figure 16: Neutral stability curves for $\beta = 0.6, 0.8, 1.0, 1.6$

Figure 17: Neutral stability curve for $\beta = 1.6$ Figure 18: The behavior of c_i of each R for $\beta = 1.6$

Figure 19: Neutral stability curves for $\beta = -0.01, 0, +0.01$ Figure 20: The behavior of c_i of each R for $\beta = 0.0$

Figure 21: Neutral stability curves for $\beta < 0$ Figure 22: Enlargement around the kink for $\beta = -0.01, -0.05$

Figure 23: The behavior of c_i of each R for $\beta = -0.1988$ Figure 24: Eigenvalue distribution by Rayleigh equation for $\beta = -0.1988$

Figure 25: Eigenvalue distribution by O-S equation for $\beta = -0.1988$ Figure 26: The behavior of c_i of each R by Rayleigh equation

References

- [1] 異友正, 後藤金英.: 数理解析とその周辺 13 「流れの線形安定性理論」, 産業図書, 1976 年
- [2] Schlichting, H.: *Boundary-Layer Theory*, Sixth Edition, McGRAW-HILL, 1968
- [3] Trefethen, L. N.: *2000 Spectral Methods in Matlab*, SIAM,
- [4] Healey, J. J.: On the neutral curve of the flat-plate boundary layer: comparison between experiment, Orr-Sommerfeld theory and asymptotic theory, *J. Fluid Mech.* (1995) vol. 288, pp.59-73.
- [5] Wazzan, A. R., Okamura, T. T. and Smith,A.M.O.: SPATIAL AND TEMPORAL STABILITY CHARTS FOR THE FALKNER-SKAN BOUNDARY-LAYER PROFILES, The Aircraft Division under sponsorship of the independent research and development program of Douglas Aircraft Company, 1 September 1968.
- [6] Orszag,S.A: Accurate solution of the Orr-Sommerfeld stability equation, *J. Fluid Mech.* **50** (1971) part 4, pp.689-703
- [7] Dongarra, J. J., Straughan, B. and Walker, D.W.: Chebyshev tau-QZ algorithm methods for calculating spectra of hydrodynamic stability problems, *Applied Numerical Mathematics*, **22**(1996), pp. 399-434
- [8] Walton, A. G.: Stability of circular Poiseuille-Couette flow to axi-symmetric disturbances, *Journal of Fluid Mechanics*, **500** (2004), pp. 169-210
- [9] Theofilis, V.: The discrete temporal eigenvalue spectrum of the generalized Hiemenz flow as solution of the Orr-Sommerfeld equation, *Journal of Engineering Mathematics* **28**(1994): pp241-259.
- [10] M.G. Macaraeg, C.L. Street and M.Y. Hussaini,: NASA TP-2858 (1988).
- [11] Jordinson, R: The flat plate boundary layer. Part 1. Numerical integration of the Orr- Sommerfeld equation, *J. Fluid Mech.* **43** (1970) pp.801-811
- [12] Asaithambi,A.: Solution of the Falkner-Skan equation by recursive evaluation of Taylor coefficients, *Journal of Computational and Applied Mathematics* 176 (2005) 203-214.